Chemical Science

ROYAL SOCIETY OF CHEMISTRY

EDGE ARTICLE

View Article Online
View Journal | View Issue

Cite this: *Chem. Sci.*, 2023, **14**, 3523

All publication charges for this article have been paid for by the Royal Society of Chemistry

Received 9th January 2023
Accepted 28th February 2023

DOI: 10.1039/d3sc00107e

rsc.li/chemical-science

Supramolecular photosensitizers using extended macrocyclic hosts for photodynamic therapy with distinct cellular delivery†

Xiuli Zheng, ‡[a] Sheng-Nan Lei,‡[a] Zekun Gao,‡[a] Xiangyu Dong,[a] Hongyan Xiao, [b] Weimin Liu, *[a] Chen-Ho Tung, [a] Li-Zhu Wu, [a] Pengfei Wang *[a] and Huan Cong *[a]

The photosensitizers (PSs) for photodynamic therapy (PDT) mostly possess conjugated skeletons that are over-sized and poorly water-soluble to be encapsulated by conventional macrocyclic receptors. Herein, we report that two fluorescent hydrophilic cyclophanes, **AnBox·4Cl** and **ExAnBox·4Cl**, can effectively bind hypocrellin B (**HB**), a pharmaceutically active natural PS for PDT, with binding constants of the 10^7 level in aqueous solutions. The two macrocycles feature extended electron-deficient cavities and can be facilely synthesized through photo-induced ring expansions. The corresponding supramolecular PSs (**HB**⊂**AnBox**$^{4+}$ and **HB**⊂**ExAnBox**$^{4+}$) exhibit desirable stability, biocompatibility, and cellular delivery, as well as excellent PDT efficiency against cancer cells. In addition, living cell imaging results indicate that **HB**⊂**AnBox**$^{4+}$ and **HB**⊂**ExAnBox**$^{4+}$ have different delivery effects at the cellular level.

Introduction

Facilitating drug delivery is crucial to achieve optimal therapeutic effects to increase drug hydrophilicity, reduce side effects, and improve bioavailability.[1,2] In particular, most photosensitizers (PSs) for photodynamic therapy (PDT) have large conjugated skeletons that are poorly soluble in water, thereby making cellular delivery of PSs an active area of investigation.[3–7] For example, the natural perylenequinonoid PS hypocrellin B (**HB**) is an active pharmaceutical ingredient in commercialized Chinese medicines for PDT treatment of skin diseases,[8,9] but is for external uses only due to its extremely low water solubility. In addition, insufficient solubility would lead to undesired aggregation which not only limits the drug delivery for biomedical applications, but also complicates the investigation to monitor and optimize the *in situ* photodynamic performance at the cellular level.[10]

Macrocycles represent a key molecular basis for supramolecular chemistry and essential resources for non-covalent interactions, thereby providing an excellent platform for drug delivery with proven success.[11–19] Compared with nanomaterial-based drug delivery strategies,[20–26] macrocyclic supramolecular receptors could form discrete, monodisperse host–guest complexes with drug molecules, featuring advantages including user-friendly operations, molecular-level precision, and guest-specific affinity.[27] Moreover, due to the reversible and dynamic host–guest interactions, macrocycles have emerged as powerful components for smart and environment-responsive drug delivery systems.[28–30]

Because of the limited cavity sizes, single molecules of conventional macrocycles, such as crown ethers, cyclodextrins, calixarenes, pillararenes, and cucurbiturils, become unsuitable to encapsulate large guest molecules with diameters of more than 1 nm like **HB**.[31,32] Thus, the suitable macrocyclic receptors for **HB** delivery should have strong guest binding to avoid drug leakage, while be able to release the PS in the cellular environment. The resulting supramolecular PS would prevent aggregate formation and multi-step chemical modifications of the natural PS.[33–38]

Here we report two water-soluble cationic cyclophanes, **AnBox·4Cl** and **ExAnBox·4Cl** (Fig. 1), as the first macrocyclic supramolecular receptors of **HB** (the natural form without chemical modifications). Both macrocycles could be facilely synthesized using an improved strategy through photo-induced ring expansions.[39–42] They feature electron-deficient hydrophobic cavities with elongated shapes to accommodate the oversized electron-rich PS and show high affinity to **HB** by forming 1 : 1 host–guest complexes with binding constants of the 10^7 level in aqueous solutions. Notably, spatiotemporal monitoring of the **HB** delivery in the cellular environment reveals that the introduction of the two

[a]*Key Laboratory of Photochemical Conversion and Optoelectronic Materials, Technical Institute of Physics and Chemistry, School of Future Technology, University of Chinese Academy of Sciences, Chinese Academy of Sciences, Beijing 100190, China. E-mail: wmliu@mail.ipc.ac.cn; wangpf@mail.ipc.ac.cn; hcong@mail.ipc.ac.cn*

[b]*Key Laboratory of Bio-inspired Materials and Interfacial Science, Technical Institute of Physics and Chemistry, Chinese Academy of Sciences, Beijing 100190, China*

† Electronic supplementary information (ESI) available: General information, synthesis and characterization, host–guest chemistry, photodynamic therapy related cell experiments, and DFT calculations. See DOI: https://doi.org/10.1039/d3sc00107e

‡ These authors contributed equally.

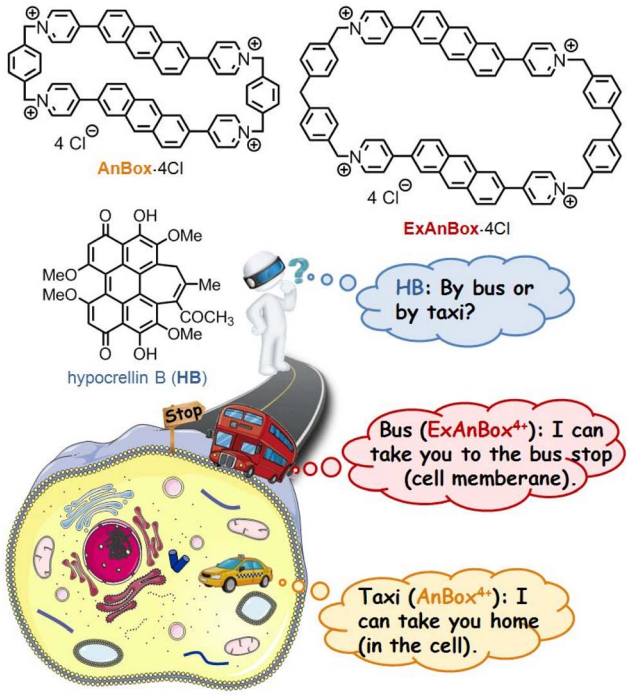

Fig. 1 Macrocycles AnBox·4Cl and ExAnBox·4Cl as supramolecular receptors of photosensitizer HB with distinct delivery effects.

macrocycles leads to high PDT efficiency against cancer cells (IC_{50} as low as 0.35 μM) with distinct delivery effects. As shown in Fig. 1, the supramolecular PS, **HB**⊂**AnBox**$^{4+}$, can enter the cells directly, while **HB**⊂**ExAnBox**$^{4+}$ leaves the macrocyclic vehicle at the cell membrane and unloads **HB** into the cells.

Results and discussion

Macrocycle design and synthesis

Because of notable features including water solubility, modifiable cavities, and electron-deficient π-conjugations, pyridinium-derived tetracationic cyclophanes[43] are promising candidates as macrocyclic hosts for the hydrophobic conjugated **HB**. In addition, we envisioned that the incorporation of polycyclic aromatic moieties (*e.g.*, 2,6-disubstituted anthracene) into the cyclophane scaffolds would not only introduce elongated cavities and fluorescent properties, but also provide extra anchors to bind **HB** through enhanced π–π interactions.[44,45] Nonetheless, conventional syntheses of the elongated cyclophanes involve consecutive nucleophilic substitution reactions (Fig. 2, the routes with grey arrows), which commonly suffer from low cyclization yields due to entropy-driven polymerization by-products. To overcome the cyclization challenges, the underexplored anthracene [4 + 4] photodimer[46–49] could serve as an X-shaped template to facilitate efficient dual cyclizations to form figure-of-eight macrocyclic intermediates, which would undergo late-stage ring expansion *via* photo-induced cycloreversion.[39–42] With this approach, the anthracene moieties can be re-installed through reversible [4 + 4] photodimerization, at the same time affording tetracationic cyclophanes with extended cavities (Fig. 2, the routes with red arrows).

Accordingly, the ring expansion approach toward **AnBox**$^{4+}$, which had been first prepared by Stoddart through consecutive nucleophilic substitutions,[50] commenced with [4 + 4]-photocycloaddition of bis(pyridyl)anthracene **1** (Fig. 2, top). The head-to-head product **4**-HH was obtained as the predominant stereoisomer likely due to the π-stacking tendency of **1**. Nucleophilic substitution between **4**-HH and bis(benzyl bromide) **2** generated the figure-of-eight intermediate **5**, forming two macrocycles in one step with 46% yield (82% yield per bond formation). Next, the photo-induced cycloreversion took place under 254 nm UV light irradiation and cleanly provided the hexafluorophosphate salt of **AnBox**$^{4+}$ with 90% isolated yield. Notably, although this ring expansion approach involves one more step than the Stoddart's route,[50] the higher overall yield reflects user-friendly purifications and improved synthetic efficiency.

Moreover, the other stereoisomer of the photodimer, the head-to-tail **4**-HT, could be amenable to the ring expansion approach toward a more extended cyclophane **ExAnBox**$^{4+}$ (Fig. 2, bottom). Because of the more flexible skeleton, synthetic attempts toward **ExAnBox**$^{4+}$ through consecutive nucleophilic substitutions merely led to a minimal isoable macrocyclization product. As such, the advantages of the ring expansion approach have been further demonstrated. Under photo-induced [4 + 4]-cycloaddition conditions, the pinacol borate-derived anthracene was preferentially converted into the head-to-tail photodimer **8** due to steric effects of the bulky substitutions. Palladium-catalyzed Suzuki–Miyaura coupling between **8** and 4-bromopyridine smoothly afforded **4**-HT. Compared to those in **4**-HH, the pyridine moieties in **4**-HT became more apart, thereby serving as matching reactive sites for longer cyclization fragments, namely the extended bis(benzyl bromide) **6**. Dual macrocyclization between **4**-HT and **6** afforded the figure-of-eight compound **9** with 40% yield (80% yield per bond formation). Likewise, the photo-induced cycloreversion of **9** generated the hexafluorophosphate salt of **ExAnBox**$^{4+}$ with 95% isolated yield. Finally, anion exchange of the hexafluorophosphate salts of **AnBox**$^{4+}$ and **ExAnBox**$^{4+}$ provided the corresponding chlorides **AnBox·4Cl** and **ExAnBox·4Cl**, respectively, as water-soluble macrocycles.

Supramolecular host–guest complexes with HB

The facile preparations through the ring expansion approach secured rapid access to sufficient amounts of both macrocycles for supramolecular characterization. Indeed, due to the extended, electron-deficient cavities, both cationic macrocycles were identified as excellent hosts for **HB** which contains oversized π-conjugation as a guest molecule. In organic solvents such as acetonitrile, proton NMR signals displayed significant shifts upon mixing **HB** and **AnBox**$^{4+}$ or **ExAnBox**$^{4+}$ hexafluorophosphate (Fig. 3). For the guest complexation of each macrocycle, one set of broadened signals were observed, indicating fast exchange of host–guest equilibrium on the NMR time scale. Specifically, the resonances of central protons of both macrocycles (positions 1–5 of **AnBox**$^{4+}$; positions 1′–5′ of **ExAnBox**$^{4+}$) were considerably shifted toward the upfield direction likely due to the shielding effect of the **HB** guest, whereas the protons at the corners of the macrocycles (positions 6,

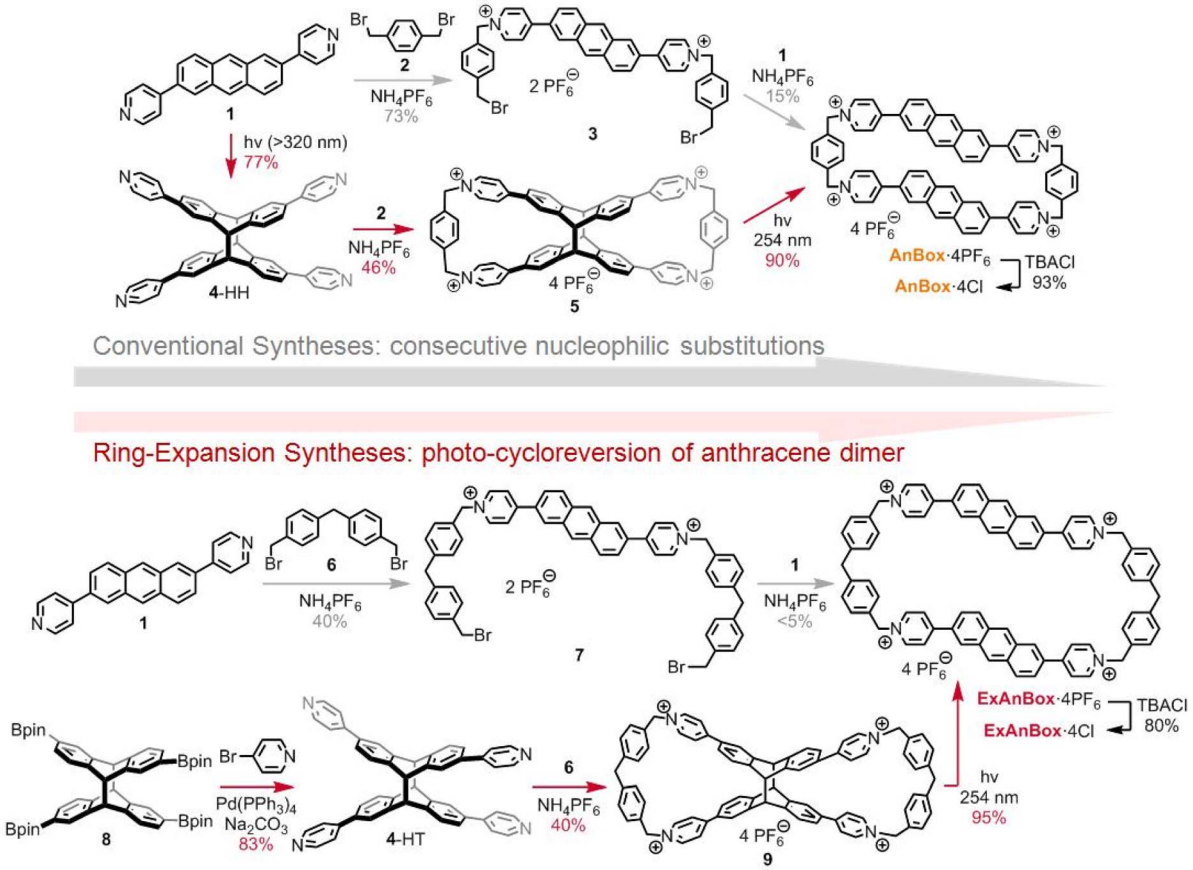

Fig. 2 Syntheses of AnBox·4Cl and ExAnBox·4Cl through photo-induced ring expansions.

7, and a of $\mathbf{AnBox^{4+}}$; positions 6′–8′, a′, and b′ of $\mathbf{ExAnBox^{4+}}$) were just slightly affected by guest inclusion. Likewise, evident upfield shifts were observed for the resonances of the aromatic protons of **HB**, with less extent of changes for those of the peripheral methoxy groups. These results are in good accordance with the inclusion of **HB** inside the macrocyclic cavities of $\mathbf{AnBox^{4+}}$ and $\mathbf{ExAnBox^{4+}}$.

Based on the **HB**-binding properties of the two macrocycles in acetonitrile, we speculated that the corresponding water-soluble macrocycles containing chloride anions would interact with **HB** more tightly in aqueous solutions because of hydrophobic effects (*cf.* Table S1†).[51] Indeed, further evidence obtained from UV-vis absorption in water suggested host–guest complex formation driven by strong non-covalent interactions, which considerably enhanced the water-solubility of **HB**. Upon addition of equimolar **HB** in the solid form to an aqueous solution of $\mathbf{AnBox^{4+}}$ (10 μM, Fig. 4a), the color of the solution changed from orange-yellow to dark red, and **HB** was completely dissolved to form a uniform solution. In parallel, the absorption of $\mathbf{AnBox^{4+}}$ at 455 nm was red-shifted to 465 nm, along with the appearance of a weak and broad band expanding to *ca.* 700 nm. By comparison, the solubility of neat **HB** is negligible in water, with the supernatant exhibiting minimal UV-vis absorption even after extended sonication (Fig. S23†). Mixing **HB** with $\mathbf{AnBox^{4+}}$ also significantly quenched the macrocycle's fluorescence intensity, which was utilized to quantitatively measure the guest binding stoichiometry and constants (Fig. 4b and c). According to fluorescence titration experiments, the mole ratio plot indicated that each $\mathbf{AnBox^{4+}}$ could bind one **HB** molecule, with a calculated binding constant of $(1.73 \pm 0.01) \times 10^7\ M^{-1}$ based on duplicate experiments. Similar results with regard to the UV-vis absorption and fluorescence changes were also observed for the other macrocycle $\mathbf{ExAnBox^{4+}}$ bearing a more extended cavity, exhibiting 1 : 1 host–guest stoichiometry and a comparable binding constant of $(1.96 \pm 0.40) \times 10^7\ M^{-1}$ in aqueous solution (Fig. 5a–c). In addition, the host–guest complexes for both macrocycles with **HB** were optimized by DFT calculations. Consistent with the NMR and photophysical characterization, the optimized structures showed that the flat **HB** molecule is surrounded by belt-like macrocycles with evident π–π interactions between the electron-rich conjugated guest and the electron-deficient central subunits of the macrocyclic hosts (Fig. 4d and 5d).

Photoactivity test and stability of supramolecular photosensitizers HB⊂AnBox^{4+} and HB⊂ExAnBox^{4+}

The chemical trapping method was applied to determine the reactive oxygen species (ROS) generation by the $\mathbf{HB}\subset\mathbf{AnBox^{4+}}$ and $\mathbf{HB}\subset\mathbf{ExAnBox^{4+}}$ complexes in response to light irradiation, employing 1,3-diphenylisobenzofuran (DPBF) and dihydrorhodamine 123 (DHR123) as singlet oxygen ($^1O_2$) and

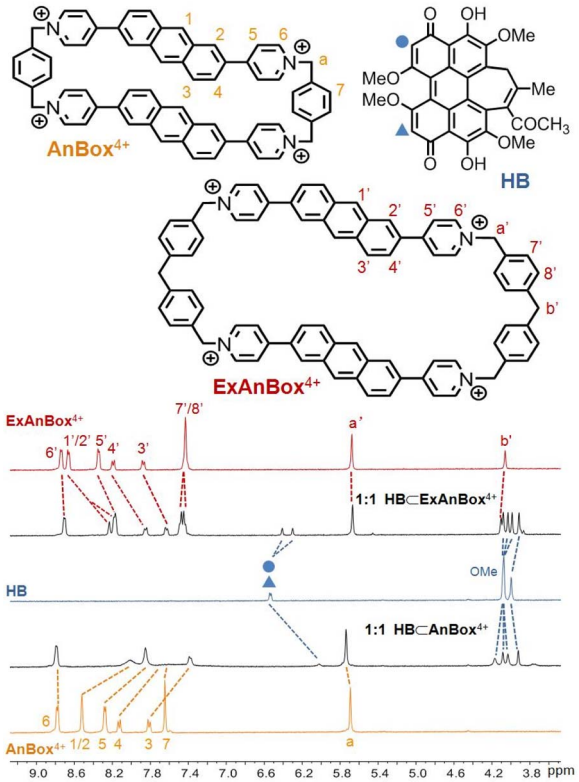

Fig. 3 Comparison of ^{1}H NMR spectra (400 MHz, CD_3CN, and 25 °C).

superoxide radical ($O_2^{\bullet-}$) trappers, respectively. As shown in Fig. 6a, in the presence of either **HB⊂AnBox^{4+}** or **HB⊂ExAnBox^{4+}**, the absorbance of DPBF at 415 nm significantly decreased at steady rates under 532 nm laser irradiation, indicating DPBF degradation as a result of $^1O_2$ generation. Furthermore, 532 nm laser irradiation could also induce evident fluorescence enhancement of DHR123 by 8.5 and 9.9 times in the presence of **HB⊂AnBox^{4+}** and **HB⊂ExAnBox^{4+}**, respectively (Fig. 6b), which suggested effective production of $O_2^{\bullet-}$. These results indicated that the two supramolecular PSs can produce both $^1O_2$ and $O_2^{\bullet-}$. Next, the stability evaluation showed that after continuous irradiation with a 532 nm laser (0.1 W cm^{-2} for 60 min), 96% and 98% of the absorbance intensities remained for **HB⊂AnBox^{4+}** and **HB⊂ExAnBox^{4+}**, respectively, suggesting excellent photo-stability for both supramolecular PSs in aqueous solutions (Fig. 6c). Moreover, the aqueous solutions of **HB⊂AnBox^{4+}** and **HB⊂ExAnBox^{4+}** can be kept under ambient conditions for at least 7 days with more than 90% of their original absorbance intensities retained (Fig. 6d), indicating negligible aggregation or degradation after extended storage.

In vitro imaging

To explore the cell uptake of the two supramolecular PSs, *in vitro* fluorescence imaging experiments using HeLa cells were performed. As control experiments, when the cells were treated with **AnBox^{4+}** or **ExAnBox^{4+}** in the absence of **HB**, obvious fluorescence signals were recorded at the cell membranes and became more

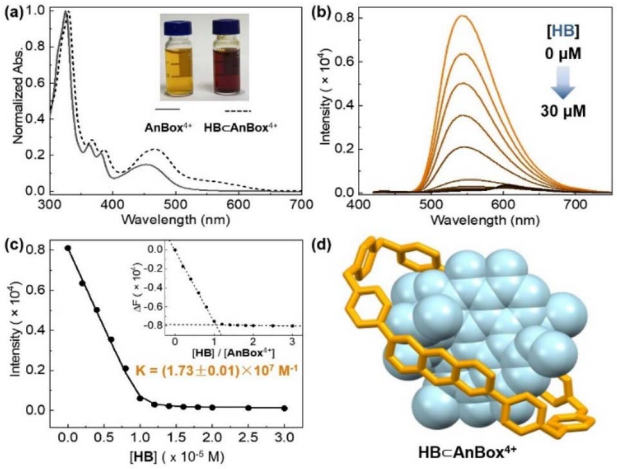

Fig. 4 Photophysical and HB-binding properties of **AnBox^{4+}**. (a) UV-vis absorption of **AnBox^{4+}** (10 μM in water) in the absence and presence of equimolar **HB** at 25 °C. (b) Fluorescence titration of **AnBox^{4+}** (10 μM in 20 : 80 DMSO/H_2O, and λ_{ex} = 350 nm) with **HB** at 25 °C. (c) Binding constant of **HB⊂AnBox^{4+}**. (Inset) Mole ratio plot indicating a 1 : 1 stoichiometry. (d) Computationally optimized host–guest complex of **HB⊂AnBox^{4+}** at the B3LYP/6-31+G* level.

intense during an extended incubation time (from 10 min to 30 min, Fig. 7a and b). At the same time, the cytoplasmic staining was not pronounced. The observed enrichment of the cationic macrocycles is consistent with their electrostatic interactions with the anionic cell surfaces. Interestingly, **HB⊂AnBox^{4+}** and **HB⊂ExAnBox^{4+}** exhibited different cellular uptake behaviors. The confocal images of HeLa cell incubated with **HB⊂AnBox^{4+}** show fluorescence throughout the cytoplasm (Fig. 7c), indicating that **HB⊂AnBox^{4+}** can easily permeate the cell membranes. Such

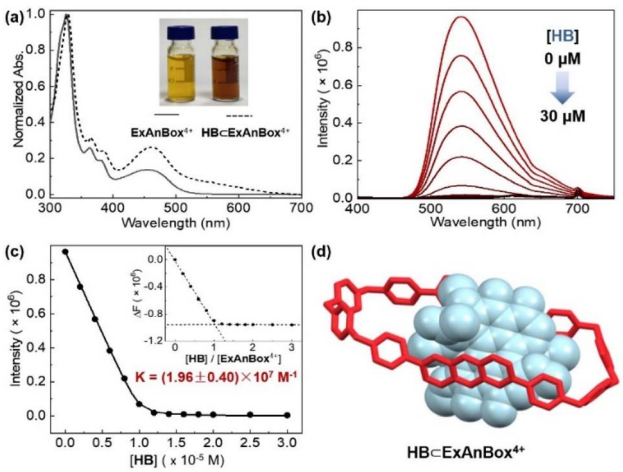

Fig. 5 Photophysical and HB-binding properties of **ExAnBox^{4+}**. (a) UV-vis absorption of **ExAnBox^{4+}** (10 μM in water) in the absence and presence of equimolar **HB** at 25 °C. (b) Fluorescence titration of **ExAnBox^{4+}** (10 μM in 20 : 80 DMSO/H_2O and λ_{ex} = 350 nm) with **HB** at 25 °C. (c) Binding constant of **HB⊂ExAnBox^{4+}**. (Inset) Mole ratio plot indicating a 1 : 1 stoichiometry. (d) Computationally optimized host–guest complex of **HB⊂ExAnBox^{4+}** at the B3LYP/6-31+G* level.

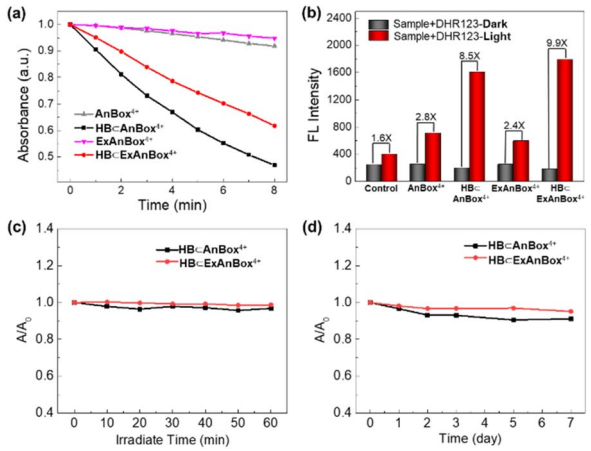

Fig. 6 (a) Normalized absorbance of DPBF at 415 nm as a function of irradiation time in the presence of **AnBox**$^{4+}$, **HB⊂AnBox**$^{4+}$, **ExAnBox**$^{4+}$, and **HB⊂ExAnBox**$^{4+}$ (20 μM in 50 : 50 DMSO/H_2O) under 532 nm laser irradiation. (b) $O_2^{\bullet-}$ detection of **AnBox**$^{4+}$, **HB⊂AnBox**$^{4+}$, **ExAnBox**$^{4+}$, and **HB⊂ExAnBox**$^{4+}$ (10 μM in water) using DHR123. (c) The photo-stability of **HB⊂AnBox**$^{4+}$ and **HB⊂ExAnBox**$^{4+}$ (10 μM in water) detected under 532 nm laser irradiation *via* absorbance spectra. (d) The stability of **HB⊂AnBox**$^{4+}$ and **HB⊂ExAnBox**$^{4+}$ (10 μM in water) detected *via* absorbance spectra.

observation was in stark contrast to the control experiments without **HB** (Fig. 7a), suggesting that the interactions between **AnBox**$^{4+}$ and **HB** should be superior to those of **AnBox**$^{4+}$ and the cell membranes. In parallel experiments, after the cells were incubated with **HB⊂ExAnBox**$^{4+}$, the fluorescence of cell membranes in the TRITC channel (mainly contributed by the signals of the macrocycles) was stronger than that in the cytoplasm, while the opposite fluorescence intensities were observed in the Cy5 channel (mainly contributed by the signals of **HB**). This result indicated that when **HB⊂ExAnBox**$^{4+}$ reaches cell surfaces, **HB** can be released from **ExAnBox**$^{4+}$ and efficiently taken up into the cytoplasm, leaving **ExAnBox**$^{4+}$ enriched in the cell membranes (Fig. 7d). The cell imaging results showed that the two supramolecular PSs have different cellular delivery behaviors for **HB** when entering the cells: **AnBox**$^{4+}$ can enter the cells together with **HB**, whereas **ExAnBox**$^{4+}$ can release **HB** at the cell membrane.

In vitro photodynamic therapy

To detect the production of ROS in HeLa cells, the fluorescence probe of dichlorofluorescein diacetate (DCFH-DA) was used. The presence of ROS can transform the weakly fluorescent DCFH-DA into its oxidized form dichlorofluorescein (DCF) with strong green fluorescence. Upon laser irradiation, the DCFH-DA + **HB⊂AnBox**$^{4+}$ and DCFH-DA + **HB⊂ExAnBox**$^{4+}$ groups showed green fluorescence signals in HeLa cells, while free DCFH-DA, free **HB⊂AnBox**$^{4+}$, and free **HB⊂ExAnBox**$^{4+}$ as controls cannot induce green fluorescence (Fig. 8a). The above results suggested that **HB** can be efficiently carried by both macrocycles and effect photodynamic ROS generation.

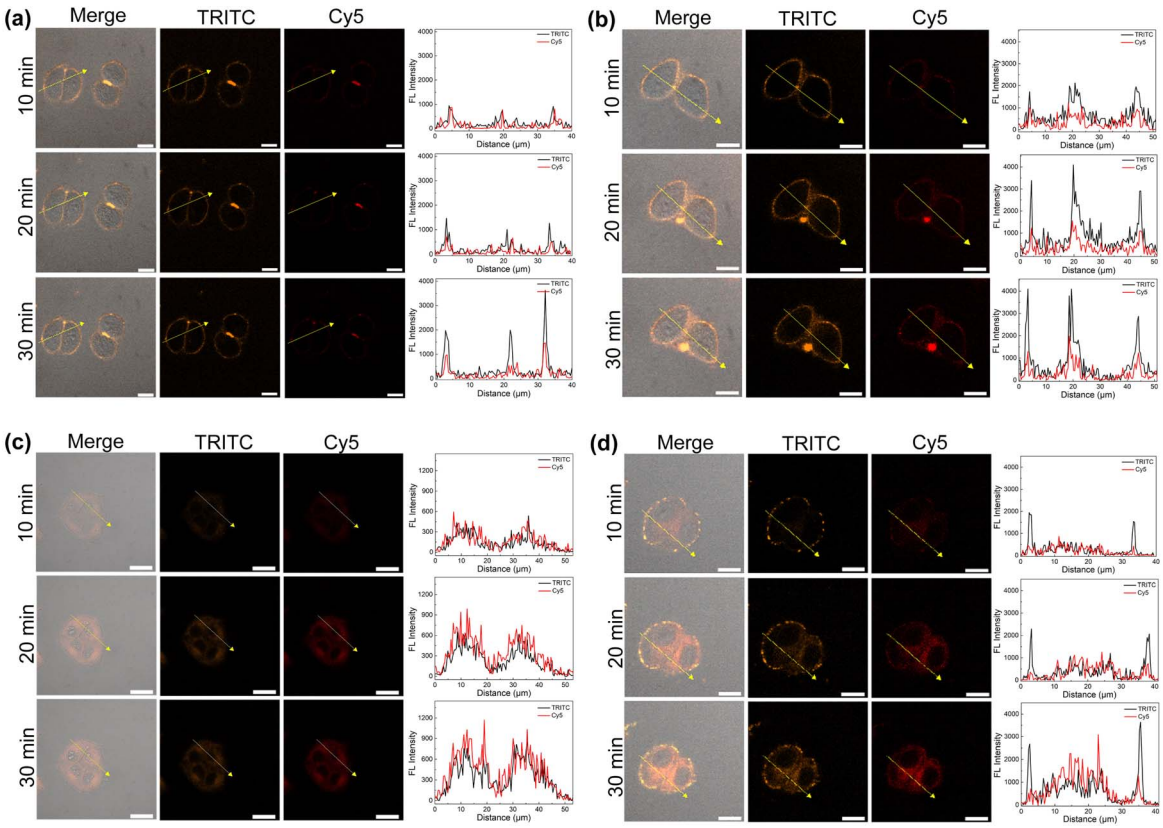

Fig. 7 Confocal images of HeLa cells incubated with (a) **AnBox**$^{4+}$, (b) **ExAnBox**$^{4+}$, (c) **HB⊂AnBox**$^{4+}$, and (d) **HB⊂ExAnBox**$^{4+}$. All concentrations are 10 μM in PBS. Scale bar: 20 μm.

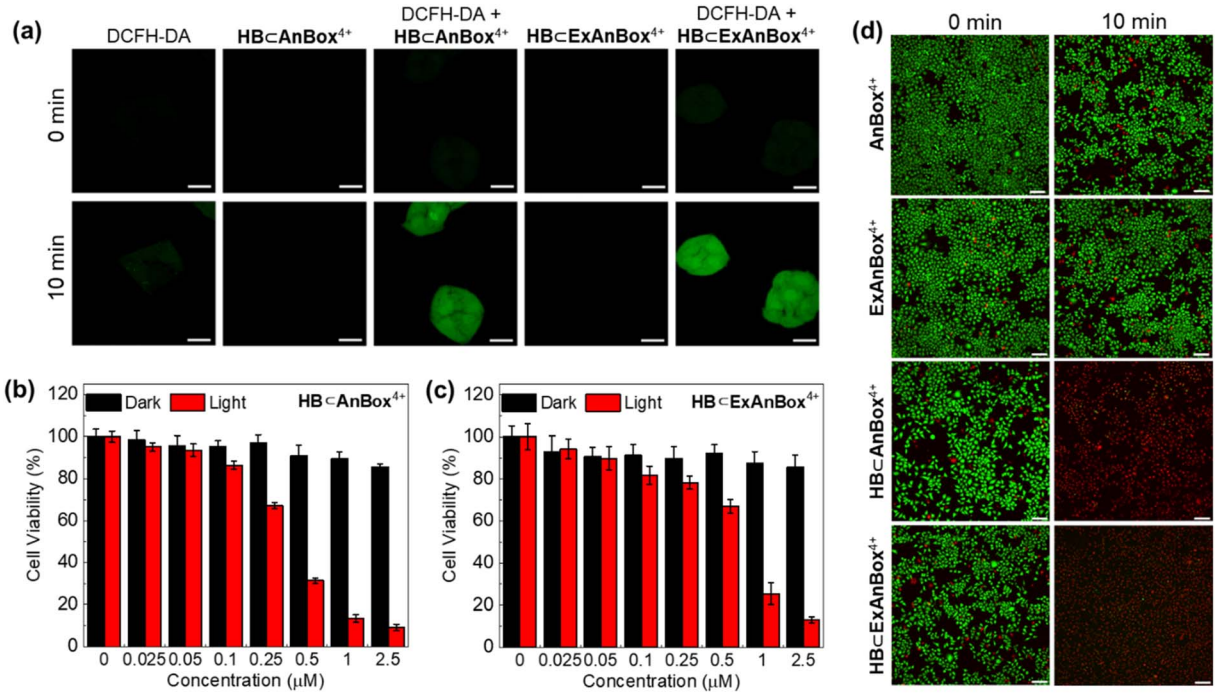

Fig. 8 (a) Fluorescence images of ROS production detected by DCFH-DA in HeLa cells. Scale bar: 20 μm. Relative viability of HeLa cells incubated with (b) **HB⊂AnBox^{4+}** and (c) **HB⊂ExAnBox^{4+}** in the culture medium in the dark or under 532 nm laser irradiation (0.1 W cm^{-2}). (d) Fluorescence images of the calcein AM and propidium iodide (PI) incubated with 2.5 μM **AnBox^{4+}**, **ExAnBox^{4+}**, **HB⊂AnBox^{4+}**, and **HB⊂ExAnBox^{4+}**, respectively, in the dark or under 532 nm laser irradiation (0.1 W cm^{-2}). Scale bar: 100 μm.

Next, the biocompatibility and photo-toxicity properties of **AnBox^{4+}**, **ExAnBox^{4+}**, **HB⊂AnBox^{4+}**, and **HB⊂ExAnBox^{4+}** against HeLa cells were evaluated by the 3-(4,5-dimethylthiazolyl-2)-2,5-diphenyltetrazolium bromide (MTT) assay. As shown in Fig. S35,† both **AnBox^{4+}** and **ExAnBox^{4+}** exhibited minimal cytotoxicity, demonstrating their high biocompatibility and low phototoxicity under 532 nm laser irradiation. Furthermore, after incubation with **HB⊂AnBox^{4+}** in the dark, the cell viability remains over 80% at 2.5 μM (Fig. 8b). Upon 532 nm laser irradiation, the photo-toxicity of **HB⊂AnBox^{4+}** becomes evident, with the cell viability reduced to 15% at 2.5 μM. The half maximal inhibitory concentration (IC_{50}) of **HB⊂AnBox^{4+}** was determined to be 0.35 μM, and that of **HB⊂ExAnBox^{4+}** (IC_{50} = 0.64 μM) is slightly higher (Fig. 8c). Calcein AM and propidium iodide (PI) co-staining assay was further used to verify the PDT efficacy by imaging live (green fluorescence) and dead (red fluorescence) cells. When irradiated with a 532 nm laser alone or treated with **HB⊂AnBox^{4+}** or **HB⊂ExAnBox^{4+}** in the dark, the cells retained a high survival rate (Fig. 8d and S36†). However, all cells died in the presence of either supramolecular PS under 532 nm laser irradiation for 10 min, which is consistent with the MTT experimental results. All of the above results indicated that **AnBox^{4+}** and **ExAnBox^{4+}** as **HB** carriers can achieve excellent photodynamic properties in living cells.

Conclusions

In summary, two fluorescent and hydrophilic cyclophanes, **AnBox·4Cl** and **ExAnBox·4Cl**, have been facilely synthesized employing a photo-induced ring expansion strategy, featuring extended macrocyclic cavities as supramolecular hosts for **HB**, an over-sized conjugated PS. Both macrocycles can make the hydrophobic **HB** soluble in water through host–guest complexation with excellent binding constants of the 10^7 level in aqueous solutions. The resulting supramolecular PSs show low toxicity in the dark, good stability, and notable photodynamic properties in living cancer cells by efficiently generating ROS under light irradiation. The fluorescent properties of the two macrocycles allow real-time monitoring of the PS delivery processes, revealing different cellular uptake behaviors of **HB⊂AnBox^{4+}** and **HB⊂ExAnBox^{4+}**. We believe that this work showcases macrocyclic carriers of over-sized PSs for effective cellular delivery and ROS generation and would inspire future development for supramolecular photodynamic therapy.

Data availability

All experimental procedures, characterization data, photodynamic therapy related cell experiments, and computational data are available in the ESI.†

Author contributions

H. C., P. W., and W. L. conceived and directed the project. X. Z., S.-N. L., Z. G., and X. D. designed and carried out the experiments. H. X. performed DFT calculations. H. C., W. L., X. Z.,

P. W., C.-H. T., and L.-Z. W. analyzed data and prepared the manuscript with inputs from all authors.

Conflicts of interest

There are no conflicts to declare.

Acknowledgements

Financial support was provided by the National Natural Science Foundation of China (21922113, 61720106014, 22088102, 21988102, and 22071257), the Chinese Academy of Sciences (XDB17000000), and TIPC Director's Fund.

Notes and references

1 J. Shi, P. W. Kantoff, R. Wooster and O. C. Farokhzad, *Nat. Rev. Cancer*, 2017, **17**, 20–37.
2 M. T. Manzari, Y. Shamay, H. Kiguchi, N. Rosen, M. Scaltriti and D. A. Heller, *Nat. Rev. Mater.*, 2021, **6**, 351–370.
3 D. E. J. G. J. Dolmans, D. Fukumura and R. K. Jain, *Nat. Rev. Cancer*, 2003, **3**, 380–387.
4 X. Zheng, J. Ge, J. Wu, W. Liu, L. Guo, Q. Jia, Y. Ding, H. Zhang and P. Wang, *Biomaterials*, 2018, **185**, 133–141.
5 C. Ji, W. Cheng, Q. Yuan, K. Mullen and M. Yin, *Acc. Chem. Res.*, 2019, **52**, 2266–2277.
6 P. C. A. Swamy, G. Sivaraman, R. N. Priyanka, S. O. Raja, K. Ponnuvel, J. Shanmugpriya and A. Gulyani, *Coord. Chem. Rev.*, 2020, **411**, 213233.
7 X. Zhao, J. Liu, J. Fan, H. Chao and X. Peng, *Chem. Soc. Rev.*, 2021, **50**, 4185–4219.
8 Q. Xiao, J. Wu, X. Pang, Y. Jiang, P. Wang, A. W. Leung, L. Gao, S. Jiang and C. Xu, *Curr. Med. Chem.*, 2018, **25**, 839–860.
9 J. Wu, J. Sha, C. Zhang, W. Liu, X. Zheng and P. Wang, *View*, 2020, **1**, 20200090.
10 Y. N. Konan, R. Gurny and E. Allémann, *J. Photochem. Photobiol., B*, 2002, **66**, 89–106.
11 X. Ma and Y. Zhao, *Chem. Rev.*, 2015, **115**, 7794–7839.
12 J. Zhou, G. Yu and F. Huang, *Chem. Soc. Rev.*, 2017, **46**, 7021–7053.
13 M. J. Webber and R. Langer, *Chem. Soc. Rev.*, 2017, **46**, 6600–6620.
14 H. Zhang, Z. Liu and Y. Zhao, *Chem. Soc. Rev.*, 2018, **47**, 5491–5528.
15 P. Li, Y. Chen and Y. Liu, *Chin. Chem. Lett.*, 2019, **30**, 1190–1197.
16 J. Wankar, N. G. Kotla, S. Gera, S. Rasala, A. Pandit and Y. A. Rochev, *Adv. Funct. Mater.*, 2020, **30**, 1909049.
17 Y.-C. Pan, X.-Y. Hu and D.-S. Guo, *Angew. Chem., Int. Ed.*, 2021, **60**, 2768–2794.
18 W. Li, W. Xu, S. Zhang, J. Li, J. Zhou, D. Tian, J. Cheng and H. Li, *J. Agric. Food Chem.*, 2022, **70**, 12746–12759.
19 Z. Wang, C. Sun, K. Yang, X. Chen and R. Wang, *Angew. Chem., Int. Ed.*, 2022, **61**, e202206763.
20 T. Sun, Y. S. Zhang, B. Pang, D. C. Hyun, M. Yang and Y. Xia, *Angew. Chem., Int. Ed.*, 2014, **53**, 12320–12364.
21 H. Cabral, K. Miyata, K. Osada and K. Kataoka, *Chem. Rev.*, 2018, **118**, 6844–6892.
22 N. Panwar, A. M. Soehartono, K. K. Chan, S. Zeng, G. Xu, J. Qu, P. Coquet, K. T. Yong and X. Chen, *Chem. Rev.*, 2019, **119**, 9559–9656.
23 J. Gao, K. Dutta, J. Zhuang and S. Thayumanavan, *Angew. Chem., Int. Ed.*, 2020, **59**, 23466–23470.
24 M. Manzano and M. Vallet-Regí, *Adv. Funct. Mater.*, 2020, **30**, 1902634.
25 N. Rohaizad, C. C. Mayorga-Martinez, M. Fojtu, N. M. Latiff and M. Pumera, *Chem. Soc. Rev.*, 2021, **50**, 619–657.
26 M. J. Mitchell, M. M. Billingsley, R. M. Haley, M. E. Wechsler, N. A. Peppas and R. Langer, *Nat. Rev. Drug Discovery*, 2021, **20**, 101–124.
27 D. Ma, G. Hettiarachchi, D. Nguyen, B. Zhang, J. B. Wittenberg, P. Y. Zavalij, V. Briken and L. Isaacs, *Nat. Chem.*, 2012, **4**, 503–510.
28 T.-X. Zhang, Z.-Z. Zhang, Y.-X. Yue, X.-Y. Hu, F. Huang, L. Shi, Y. Liu and D.-S. Guo, *Adv. Mater.*, 2020, **32**, 1908435.
29 Y.-M. Zhang, Y.-H. Liu and Y. Liu, *Adv. Mater.*, 2020, **32**, 1806158.
30 W.-C. Geng, J. L. Sessler and D.-S. Guo, *Chem. Soc. Rev.*, 2020, **49**, 2303–2315.
31 F. Schmitt, J. Freudenreich, N. P. Barry, L. Juillerat-Jeanneret, G. Suss-Fink and B. Therrien, *J. Am. Chem. Soc.*, 2012, **134**, 754–757.
32 I. Roy, S. Bobbala, R. M. Young, Y. Beldjoudi, M. T. Nguyen, M. M. Cetin, J. A. Cooper, S. Allen, O. Anamimoghadam, E. A. Scott, M. R. Wasielewski and J. F. Stoddart, *J. Am. Chem. Soc.*, 2019, **141**, 12296–12304.
33 K. Liu, Y. Liu, Y. Yao, H. Yuan, S. Wang, Z. Wang and X. Zhang, *Angew. Chem., Int. Ed.*, 2013, **52**, 8285–8289.
34 J. Gao, J. Li, W.-C. Geng, F.-Y. Chen, X. Duan, Z. Zheng, D. Ding and D.-S. Guo, *J. Am. Chem. Soc.*, 2018, **140**, 4945–4953.
35 X. Li, S. Lee and J. Yoon, *Chem. Soc. Rev.*, 2018, **47**, 1174–1188.
36 H.-T. Feng, Y. Li, X. Duan, X. Wang, C. Qi, J. W. Y. Lam, D. Ding and B. Z. Tang, *J. Am. Chem. Soc.*, 2020, **142**, 15966–15974.
37 K. Yang, Z. Zhang, J. Du, W. Li and Z. Pei, *Chem. Commun.*, 2020, **56**, 5865–5876.
38 N. Kwon, H. Kim, X. Li and J. Yoon, *Chem. Sci.*, 2021, **12**, 7248–7268.
39 Z.-A. Huang, C. Chen, X.-D. Yang, X.-B. Fan, W. Zhou, C.-H. Tung, L.-Z. Wu and H. Cong, *J. Am. Chem. Soc.*, 2016, **138**, 11144–11147.
40 Z. Zhao, Q. Zhu, Z. Wang, J. Lu, Z. Jin and H. Liu, *Macromolecules*, 2017, **50**, 8907–8915.
41 W. Xu, X.-D. Yang, X.-B. Fan, X. Wang, C.-H. Tung, L.-Z. Wu and H. Cong, *Angew. Chem., Int. Ed.*, 2019, **58**, 3943–3947.
42 Y. Ueda, K. Suzuki and K. Ohmori, *Org. Lett.*, 2020, **22**, 2002–2006.
43 X.-Y. Chen, H. Chen and J. F. Stoddart, *Angew. Chem., Int. Ed.*, 2023, **62**, e202211387.

44 E. J. Dale, N. A. Vermeulen, M. Juricek, J. C. Barnes, R. M. Young, M. R. Wasielewski and J. F. Stoddart, *Acc. Chem. Res.*, 2016, **49**, 262–273.
45 I. Roy, A. H. G. David, P. J. Das, D. J. Pe and J. F. Stoddart, *Chem. Soc. Rev.*, 2022, **51**, 5557–5605.
46 H. D. Becker, *Chem. Rev.*, 1993, **93**, 145–172.
47 H. Bouas-Laurent, J.-P. Desvergne, A. Castellan and R. Lapouyade, *Chem. Soc. Rev.*, 2001, **30**, 248–263.
48 C. Yang and Y. Inoue, *Chem. Soc. Rev.*, 2014, **43**, 4123–4143.
49 W. Liu, L. Guo, Y. Fan, Z. Huang and H. Cong, *Chin. J. Org. Chem.*, 2017, **37**, 543–554.
50 A. Garci, Y. Beldjoudi, M. S. Kodaimati, J. E. Hornick, M. T. Nguyen, M. M. Cetin, C. L. Stern, I. Roy, E. A. Weiss and J. F. Stoddart, *J. Am. Chem. Soc.*, 2020, **142**, 7956–7967.
51 A. Gu and N. J. Wheate, *J. Inclusion Phenom. Macrocyclic Chem.*, 2021, **100**, 55–69.